

Article

The Light-Trapping Character of Pit Arrays on the Surface of Solar Cells

Baohua Zhu ^{1,2}, Le Chen ^{1,*}, Song Ye ^{1,*}  and Wei Luo ¹

¹ Guangxi Key Laboratory of Optoelectronic Information Processing, School of Optoelectronic Engineering, Guilin University of Electronic Technology, Guilin 541004, China

² School of Materials Science and Engineering, Guilin University of Electronic Technology, Guilin 541004, China

* Correspondence: chenle11@126.com (L.C.); yesong@guet.edu.cn (S.Y.)

Abstract: Surfaces with light-trapping structures are widely used in solar cells to enhance light capturing and to transform efficiency. The study of light-trapping character is important for light-trapping structures in solar cells. In the present study, the light-trapping character for the regular hemisphere pit arrays (RHPAs) in solar cells was intensively investigated in terms of reducing light reflection, suppressing light escape, and increasing the length of the optical path. Results show that the RHPAs can decrease surface reflectivity by ~54% compared with the plane structure, and can reflect ~33% of the light that has not been absorbed back into the absorption layer of the solar cell. The total optical path of the cell with the RHPAs structure remarkably increased from 2ω to 4ω . To verify the theoretical research conclusions, we produced the glass structure samples with different aspect ratios by using micro/nanometer-processing technology. The reflection ratios for silicon wafers covered by plane and RHPAs glass samples were tested. The test results were compared with the theoretical calculation results, which showed consistency.

Keywords: light-trapping character; regular hemisphere pit arrays (RHPAs); anti-reflection; optical path length



Citation: Zhu, B.; Chen, L.; Ye, S.; Luo, W. The Light-Trapping Character of Pit Arrays on the Surface of Solar Cells. *Photonics* **2023**, *10*, 855. <https://doi.org/10.3390/photonics10070855>

Received: 31 May 2023
Revised: 28 June 2023
Accepted: 29 June 2023
Published: 24 July 2023



Copyright: © 2023 by the authors. Licensee MDPI, Basel, Switzerland. This article is an open access article distributed under the terms and conditions of the Creative Commons Attribution (CC BY) license (<https://creativecommons.org/licenses/by/4.0/>).

1. Introduction

Photovoltaic energy has broad prospects for green energy development. However, compared with traditional energy resources, solar energy experiences deficiencies such as high manufacturing cost and unideal transform efficiency, which seriously limit its wide application. To improve the conversion efficiency, researchers have developed light-trapping structures for various solar cells, such as nano/micro-pyramids [1–4], nanowires [5–7], nanocone [8–12], nanosphere [13–16], and porous silicon structures [17,18]. Light-trapping structures possess broadband optical absorption abilities, which can effectively lower the loss of light caused by reflection and raise the valid length of optical paths in the active layer of solar cells [19]. The fabrication of the trapping structures often relies on the relatively expensive micro-nano processing technology, such as lithographic development, dry and wet etching, and reactive ion etching. Considering that the processes are often manufactured internally within the solar cells, it is easy to damage the primitive structure, which may reduce the lifetime of the devices. Therefore, the prospect of scaled production of the light-trapping structures prepared inside the cells remains uncertain.

Surface light-trapping technology has been proposed for the significant improvement with two distinct advantages of high reliability and non-disruption of the devices. Quarter-wavelength anti-reflection (AR) coating is among the most common surface light-trapping technologies, which has been widely used for different types of photovoltaic devices or modules [20–23]. However, its conversion effectiveness is dependent on wavelength and the angle of incidence. The preparation of efficient multistory AR coatings is also inseparable from many complex chemical and physical processes, such as sol-gel and magnetron sputtering. Alternative technology is based on a low-cost, flexible, polydimethylsiloxane

(PDMS) thin film, which is processed into 3D nanopit and covered in the outer face of the solar cell without a binding agent [24,25]. Experimental results show that the PDMS thin membrane has superb anti-reflection performance and can be applied to many types of solar cell to promote the transform efficiency. However, the absorption of incident light by the PDMS and the air stored between the PDMS and solar cell may result in wasted light energy. In addition, SiO₂ microparticles with distinct optical characteristics are also attractive [26–29]. It can effectively increase the light absorption through proper arrangement on the cell surface. SiO₂ hemisphere texture surface shows a perfect function and prospect in the application field of high-efficiency photovoltaic cells. However, the preparation of large-area and uniform SiO₂ microsphere surfaces on the surface of the solar cell is difficult.

A novel and efficient surface-trapping technology has attracted the attention of researchers. Wang et al. used an effective light-coupling method, in which a periodic quasi-hemisphere micro-nanostructure was prepared on the front glass surface to improve the property in thin-membrane solar cells [30–32]. This process does not require a change in the processing technology of thin-film solar cells with a flat glass substrate. Experimental results show that the pit arrays have good light-trapping properties in the solar cell, particularly for Si thin-membrane solar cells, including single and tandem solar cells. Shen et al. have reported that, compared with the classical plane surface solar cell, the efficiency of the surface of an a-Si:H/ μ c-Si:H tandem solar cell of periodic pit array increased from 11.67% to 12.23%, and the short-circuit current density (J_{sc}) increased by 4.6%. In the present study, compared with the flat cell, the trapping structure of hemispherical pit arrays can increase the transformation efficiency by ~6% and the short-circuit current by ~7% for a single a-Si:H thin-film solar cell with a textured surface. The surface with periodic micro-structured arrays has shown good light-capture properties in solar cells. Although there have been many reports on the trapping mechanism of light-trapping structures in solar cells [33–35], there is still a lack of in-depth theoretical research on the surface-trapping mechanism, especially on the surface of the light-capture mechanism. The light-capture mechanism is important for further understanding the nature of the light capture and ameliorating the high-efficiency light-capture structures for solar cells. In this work, numerical analyses and geometrical optics simulations were carried out to investigate the light-capture mechanism of surface pit arrays with different aspect ratios in silicon solar cells, including anti-reflection characteristics, overall reflection ratio, and overall length of light path. Moreover, the theoretical research conclusions were verified by manufacturing the glass structure samples by using micro/nanometer-processing technology. The reflection ratios of silicon wafers covered by the plane and RHPAs glass samples were measured for comparison. Lastly, theoretical calculations were carried out for comparison with the experimental measurements.

2. Fabrication and Simulation of the RHPA Structures

2.1. Fabrication Process and Characterization

Figure 1 shows a thin-film silicon solar cell with the RHPAs on its surface, and a quasi RHPA structure was fabricated on smooth quartz glass. First, a 3-inch optical glass was washed with ethanol and acetone, and then boiled at 180 °C in the admixture of dense H₂SO₄ and H₂O₂ with bulk ratio of 3:1 for the removal of various residual organic matter. Second, a semispherical pit array structure was fabricated on an optical glass by using various types of micro-nanometer processing techniques, including UV lithography, the sputtering of metal seed mask, HF (buffered hydrofluorocarbon acid solution) etching, and ion beam etching. Figure 2 schematically shows the key fabrication process. The pit array's depth and period (the distance between two adjacent pits) could be improved by altering the isotropical etching time in the HF solution and the mask size. A mask with a period of 10 μ m and diameter of 2.5 μ m was used, because a 10 μ m feature size structure can obtain a better aspect ratio of the pit arrays and meet the spectral range of the solar cell to absorb light.

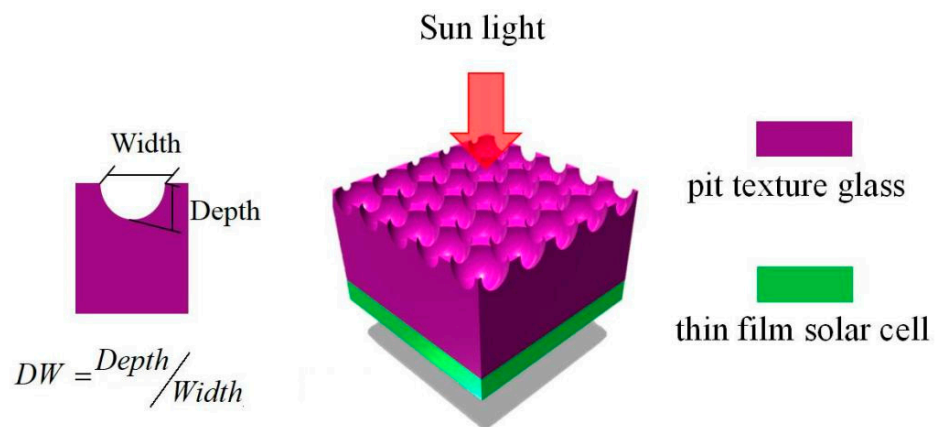


Figure 1. Schematic diagram of the thin-film Silicon solar cell with regular pit arrays.

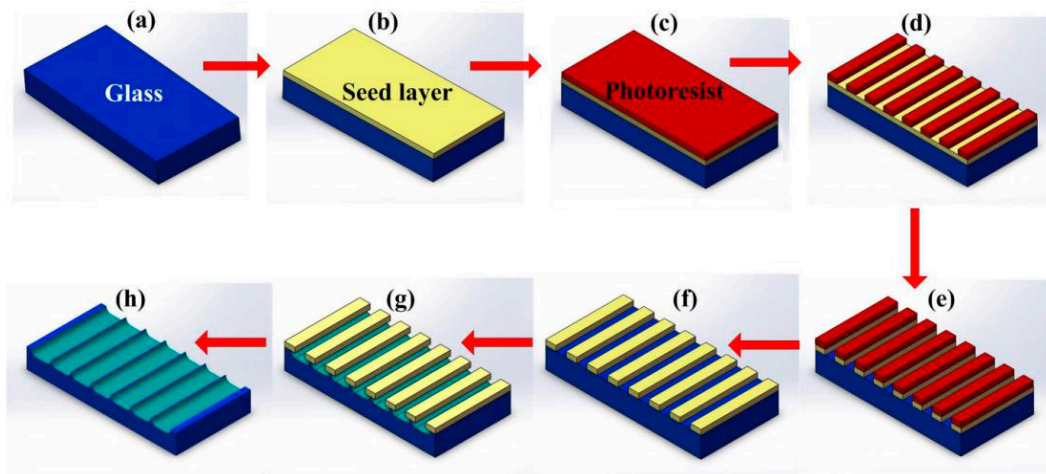


Figure 2. Schematic of key fabrication process of regular pit arrays on glass substrate: (a) washing glass substrate; (b) sputtering metal seed layer; (c) spinning photoresist layer; (d) lithography and developing; (e) etching metal layer; (f) moving photoresist; (g) etching glass with HF solution; (h) removing metal seed layer.

Notably, the aspect ratio ($DW = \text{Depth}/\text{Width}$) of the pit array is equal to or below 0.5 ($DW \leq 0.5$) owing to the isotropic properties of glass materials. Thus, the ultimate RHPA prepared from the above-mentioned approach is a quasi-hemisphere pit array ($DW \approx 0.45$). If the pit structure with high aspect ratio ($DW \geq 0.5$) needs to be prepared on the surface of the glass, the combined processing of HF etching and reactive-ion etching (RIE) needs to be carried out. First, RIE was used to prepare the high-aspect-ratio pit arrays, and then HF etching was carried out to obtain the smooth surface. Other processes are similar to those as described above.

The morphology of the RHPAs' glass experimental products was observed using a field emission scanning electron microscope. The transmission spectrum and light reflection ratio were observed using a UV-vis-NIR spectrophotometer.

2.2. Simulation of Optical Transmission Property

The optical transmission property for the structure of RHPAs in solar cells was studied by using the particle tracing module of COMSOL Multiphysics. For the convenience of research, during the simulation process, the refractive indices of Si, air, and glass were set to 3.5, 1, and 1.5, respectively. At the same time, the imaginary part of their refractive indices was ignored, and the incident optical wavelength was set to 650 nm. The process of light propagation was visualized using a hemispherical pit model (radius = 1, dimensionless) for simulating the propagation of light in the RHPAs. Furthermore, the reflectivity,

transmittance, scattering rate, and light path length were calculated using the Visual Basic (VB) program.

3. Light-Trapping Mechanisms and Discussions

Figure 3 shows the light transmission properties in a solar cell model with the RHPAs' surface, in which the aspect ratio was $DW = 0.5$. It shows that the hemisphere of the RHPAs can achieve partial incident light re-absorption via the total reflection inside pit arrays. It also depicts that the light incident from region I ($0 < x < 0.5$), where x is the distance from the center of the pit, cannot be trapped in the pit, as shown in Figure 3a. However, the light from the II ($0.5 \leq x < 0.81$) or III ($0.81 \leq x \leq 1$) area can be adjusted using the refraction and total internal reflection of the side of the pit to achieve a two- and three-fold increase in light injection, respectively. The repeated injection of the incoming optical evolved the total reflectance (R) of the solar cells to R^k , where k is a multiple of the injection. The PHRAs' structure can scatter the incident light and enter the solar cells at a certain angle, as shown in Figure 3b. It is beneficial for improving the light path in the cells. The other significant property of RHPAs is that they may return the light that has not been absorbed to the absorbing layer once more. As shown in Figure 3c, when the internal optical ray is transmitted from the glass to the air, if the ray does not meet the requirements of total reflection ($\theta < \theta_c$), the glass would stop it, whereas when $\theta > \theta_c$, the optical ray would be reflected by the RHPAs and would return to the active layer, where θ is the incident angle, and θ_c is the critical angle of total reflection. Therefore, the light-trapping mechanism of the RHPAs can be summarized in terms of reducing light reflection, suppressing light escape, and increasing optical path length, as shown in Figure 3d. Each aspect of the mechanisms was investigated as detailed in the following sections.

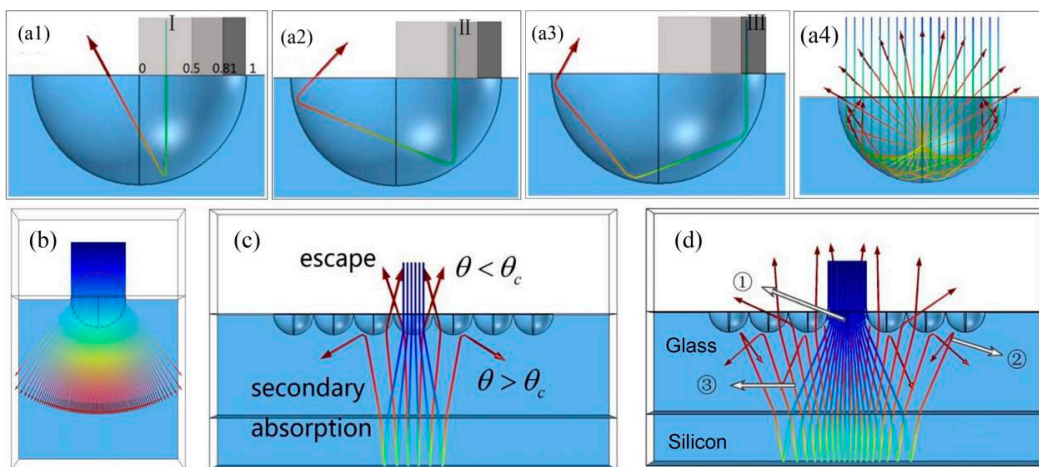


Figure 3. Transmission properties of light in a solar cell model with RHPA surface. The reflection path of incoming rays in area I (a1), II (a2), and III (a3), and a view of the whole reflection (a4). (b) Scattering light of the hemisphere pit. (c) Transmission or reflection path of rays hitting from itself to the RHPAs. (d) PHRAs' total light capture mechanism in the solar cell.

(a) Reducing Light Reflection

Generally, the surface reflectivity of glass is ca. 4%. However, if the light can be reflected twice, the reflectivity will reach as low as 0.16%. The higher the time of reflection, the lower the reflectivity is. The hemispherical pit's radius was set to 1. Accordingly, the critical conditions for multiple incidence could be determined with programming calculations, and the schematic diagram is shown in Figure 4, where r_I , r_{II} , and r are the critical conditions when light is injected into the cell the first, second, and greater than or equal to the third time with values of 0.5, 0.81, and 1, respectively. The corresponding

areas of $S_I = \pi r_I^2$, $S_{II} = \pi(r_{II}^2 - r_I^2)$, and $S_{III} = \pi(r^2 - r_{II}^2)$ are r_I , r_{II} , and r , respectively. Therefore, for the hemisphere pit arrays, the surface reflectance is as follows:

$$R_{hemisphere} = \left(\frac{S_0 - S}{S_0} + \frac{S_I}{S}\right)R^1 + \frac{S_{II}}{S}R^2 + \frac{S_{III}}{S}R^3 = 0.4625R + 0.406R^2 + 0.3439R^3 \quad (1)$$

where R is the reflection coefficient of the glass, $S = \pi r^2$ is the total area of the hemisphere pit, and $S_0 = (2r)^2$ is the area of the square cell. For glass with a refractive index $n = 1.5$, $R \approx 0.04$, which is much less than 1. At $r = 1$, $R_{hemisphere} \approx 0.4625R = 0.0185$, indicating that the hemispherical pit structure model can reduce surface reflectance by more than half (~54%) compared with the flat structure. In the actual structure, its surface reflectance may be lower. Thus, the hemisphere pit arrays can reduce the light reflection and capture the majority of the optics into solar cells.

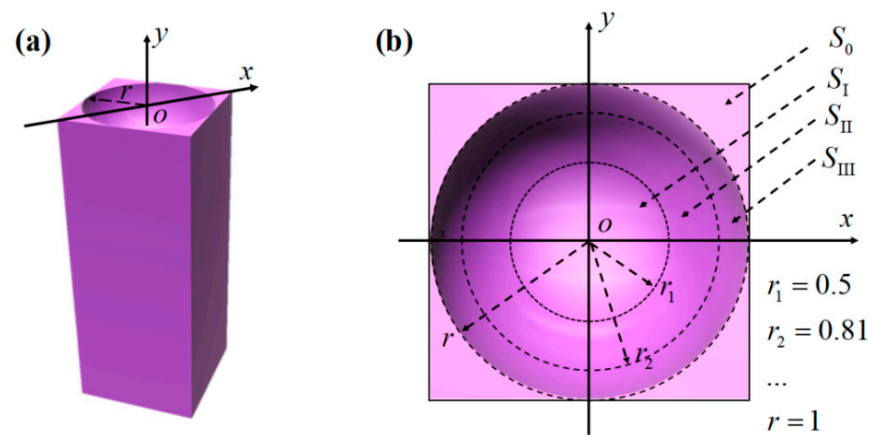


Figure 4. (a) Mathematical and physical model of the hemispheric pit. (b) The schematic diagram of the interaction between the incident light in different regions and the hemispherical pit structure.

(b) *Suppression of Escaped Light*

In solar cells, escaping light is another crucial problem. The suppression of escaped light will further enhance the absorption of incoming light. When light arrives at the active layer of solar cells through the glass, it interacts with the active layer or becomes reflected back into the air. The more light that is not absorbed or reflected, the lower the conversion efficiency of the cell. Otherwise, the efficiency will be improved. Therefore, surface-trapping technology is expected to play an active role in this aspect. The RHPA structure plays such an important role because it can return part of the unabsorbed light back to the active layer once more. When internal light is transmitted from the glass to the air, if the light does not reach the requirements of total reflection, it will stop at the glass. Otherwise, it will be reflected into the solar cell again. The critical angle is $\theta_C = 41^\circ$, when the indexes of refraction of air and RHPAs were $n_{air} = 1$ and $n_{RHPAs} = 1.5$, respectively.

Figure 5a shows the diagrammatic sketch of the optical ray in the RHPAs with $DW = 0.5$. It is assumed that the entire optical ray will be totally reflected at the bottom of the RHPAs. When the internal optical ray is transmitted from the RHPAs to the air, it will stop the RHPAs if $\theta < \theta_C$. By contrast, the optical ray would be reflected by the RHPAs and returned to the active layer of the cells again. Based on the total reflection theorem, by using the VB programming method, the quantitative relationship among incoming, transmission, and reflection light was calculated, and the results are shown in Figure 5b. In the figure, p_{tra} and p_{ref} represent the percentage of transmission light and reflection light of each position in all incoming light, respectively. By using the integral method, the probability of total reflection and total transmission was obtained as follows:

$$S_{ref} = \int_{x=0}^{\infty} P_{ref} dx = 64.66 \text{ and } S_{tra} = \int_{x=0}^{\infty} P_{tra} dx = 129.51 \quad (2)$$

$$P_{total-ref} = \frac{S_{ref}}{S_{tra} + S_{ref}} = 33.21\% \text{ and } P_{total-tra} = \frac{S_{tra}}{S_{tra} + S_{ref}} = 66.79\% \quad (3)$$

where S_{ref} and S_{tra} are the weighted integral of the area of p_{ref} and p_{tra} , and $P_{total-ref}$ and $P_{total-tra}$ are the probability of total reflection and total transmission, respectively. Therefore, the hemisphere RHPAs can return 33.21% of the light that has not been absorbed to the absorbing layer once more. This unabsorbed light will be absorbed for a second time. The probability of light that escapes directly without being absorbed is 66.79%, and this part of light escapes directly. These important data show that about 30% of light recycling can be obtained by the hemisphere RHPAs. Therefore, RHPAs can impede the escaping light and enhance the utilization of incoming light as the second aspect of the light-trapping mechanism in this investigation.

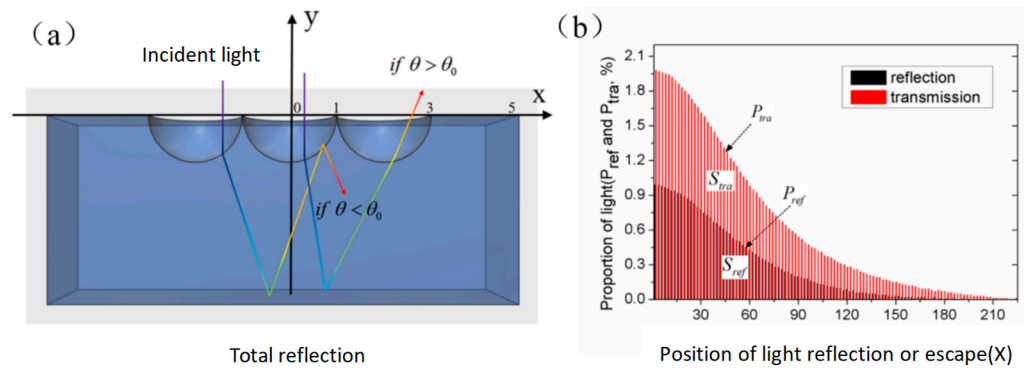


Figure 5. (a) (Total reflection.) The diagrammatic sketch of optical rays in RHPAs. (b) (Position of light reflection or escape (X).) The diagrammatic sketch of the percentage of transmitted light and reflected light of each position for all incoming light.

(c) Increasing Light Path Length

In addition, RHPAs can scatter light and raise the propagation length of optical rays in the active layer. Reference [36] studied the absorption layer conditions in an ideal suede structure [36], and referring to the physical ideas within it, we will discuss the degree of increase in optical path of silicon thin-film solar cells caused by the hemisphere RHPAs' structure relative to plane structure. Figure 6a shows the propagation of the optical ray in the cell model with RHPAs. Figure 6b shows the comparison of light propagation in the cell model of the plane structure and the cell model of RHPAs, where x_0 represents the point of incidence of light, θ_1 is the incident angle in glass, θ_2 is the refracted angle in the cell, and θ_3 is the scattering angle in Si. The l_{opt} represents the propagation length of the incident optical ray in the silicon layer, ω represents the silicon thickness, and d represents the glass thickness. The values $n_1 = 1$, $n_2 = 1.5$, and $n_3 = 3.5$ were chosen as the refractive index of air, glass, and silicon, respectively. Figure 6c shows the mathematical relationship between x_0 , ω , and l_{opt} . As shown in Figure 6d, the relationship between θ and x_0 and the relationship between l_{opt} and x_0 were observed.

In summary, and combined with statistical methods, the average optical scattering angle and optical path length can be obtained using the following formula:

$$\langle \theta \rangle = \frac{1}{j} \sum_{i=1}^j \theta_3 = 6.67^\circ \text{ and } \langle l_{opt} \rangle = \frac{1}{j} \sum_{i=1}^j l_{opt} = 1.0069\omega \quad (4)$$

The scattering angle θ increased with the change in incident position x_0 . However, considering that Si has a much higher refractive index than glass, the scattering angle varied from 0 to 20°. Accordingly, an average scattering angle of 6.67° was obtained. Similarly, the optical path of scattered light l_{opt} will also change with the location of incoming light. However, it is relatively limited in increasing the propagation length of light according to

the incoming position of light, and the increase will be in evidence only near the pit edge. Therefore, the average optical path of scattering light is about 1.0069ω .

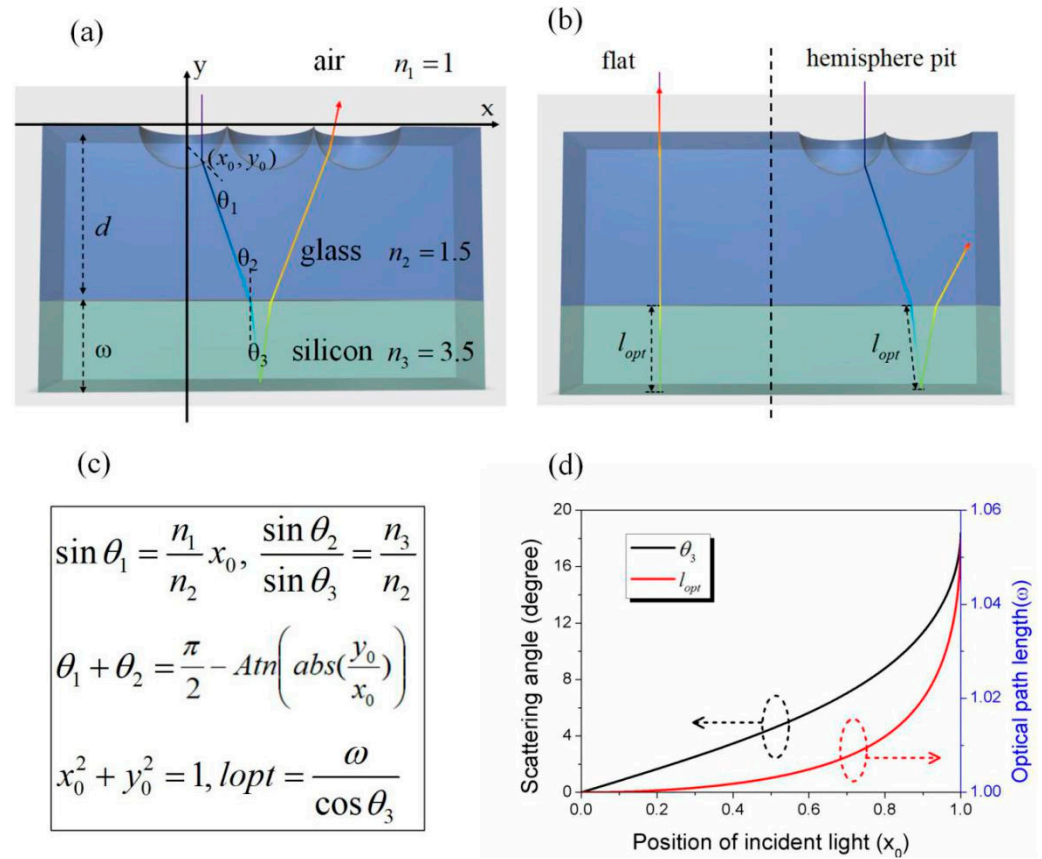


Figure 6. (a) The diagram of propagation of the optical ray in the pit texture cell. (b) The comparison diagram of light propagation in the plane structure cell and the pit texture structure cell. (c) The conversion relationship among light incident positions, cell thickness, and light path length. (d) The relationship between scattering angle and incident light position, and the relationship between the optical path and the incident light position.

The above analysis about the optical path and the probability of transmission and reflection was synthesized, and the Lambert surface method can be used to estimate the total optical path length of light in solar cells, which is also a relatively reasonable method [37,38].

$$L_{opt} = \sum dl_{opt} = 2l_{opt} + p_{tra}l_{opt} + 3p_{tra}p_{ref}l_{opt} + 5p_{tra}p_{ref}^2l_{opt} + \dots \quad (5)$$

For hemisphere pit arrays, $P_{ref} = 33.21\%$ and $l_{opt} = \langle l_{opt} \rangle = 1.0069\omega$, Equation (5) is convergent:

$$L_{opt} \approx 4\omega \quad (6)$$

The above calculation results indicate that the total optical path length is increased from initial 2ω to 4ω by the hemisphere pit arrays. Therefore, the light transmission length in RHPAs has risen twice compared with the plane structure glass. Compared with the textured structure inside the solar cell, the limited raise in light propagation length is not obvious for improving the transform efficiency of solar cells, but it has provided rare opportunities and favorable space for reducing the active layer thickness and saving manufacturing expense for cells.

4. Experimental Verification

The light-trapping mechanism of RHPAs is mainly characterized via reduce surface reflectivity for solar cells, because RHPAs can refract and reflect incoming light multiple times before it reaches the active layer of the solar cell. Experimental methods were employed to compare the total reflection capability of solar cells with flat panel and RHPA structures. To verify the theoretical research results, the above-mentioned manufacturing method was used to obtain a PDMS film with flat and RHPA structures.

Figure 7a1,a2 shows the photograph of the quasi-hemispherical pit array textured glass and its diffraction pattern with the laser beam (500 nm) passing through. The diffraction pattern illustrates outstanding regular surface and superior diffraction result of the textured glass sample. Figure 7 shows the scanning electron microscope image of RHPA glass (inclination angle, 30). The pit array has a period of about 20 μm and an aspect ratio of about 0.5. Figure 7c shows the SEM images of the pits at different aspect ratios. Figure 7d provides a comparison of the reflectivity spectrum of flat and textured glass samples. The transmissivity for the quasi-PHRA glass has altered greatly compared with the plane glass. When the light passed through the surface structure, the transmissivity increased by several percent. However, when the light came into the surface structure from the inverse side, the transmissivity decreased to 70–75%. Figure 7e illustrates the light reflection feature of a silicon wafer-covering glass with a quasi-hemisphere pit array structure, and shows a comparison with plane glass. Based on the diagram, the total reflectance of the Si wafer covered by the PDMS film is as follows:

$$R_{total} = R_1 + R_2 \tag{7}$$

For the flat glass sample (without the RHPA structure),

$$R_{1-flat} = \left(\frac{n_{glass} - n_{air}}{n_{glass} + n_{air}} \right)^2, R_{2-flat} = \left(\frac{n_{Si} - n_{glass}}{n_{Si} + n_{glass}} \right)^2 \tag{8}$$

Meanwhile, for the textured glass sample (with the RHPA structure),

$$R_{1-RPAs} = 0.4625R_{1-flat}, R_{2-RPAs} = 0.3321R_{2-flat} \tag{9}$$

where n_{air} represents the air refractive index, n_{glass} represents the glass refractive index, and n_{Si} represents the Si refractive index.

Figure 7f expresses the silicon wafer theory and experiment reflectivity for samples separately covered with plane and hemisphere-pit-array glass when light with a wavelength of 350–800 nm is vertically incident. In order to reduce the impact of the air layer between the silicon and the structured glass on the test results, we introduced a refractive-index-matching solution between the silicon and the structured glass. In order to eliminate the influence of the air layer between the silicon and the structured glass on the test results, we introduced refractive index matching between the silicon and the structured glass, which was prepared with ethanol C₂H₅OH, liquid paraffin, and sodium bromide C₁₀H₇Br in a ratio of 1:1:1. The refractive index was equivalent to that of glass, about 1.5. The small image inserted in the figure is the refractive index curve of the silicon wafer used in the theoretical calculations of this section.

It shows that the theoretical and experimental results are in agreement. Notably, in the theoretical calculation, a strict hemisphere model was obtained, but in the experiment, only a quasi-hemispherical model was used. The aspect ratio of the quasi-hemisphere is ca. 0.45. In the theoretical calculations, the refractive indexes of Si were related to wavelength, which is the famous optical database refractive index [39,40]. In the theoretical calculations, the refractive index of the matching solution is taken as 1.5.

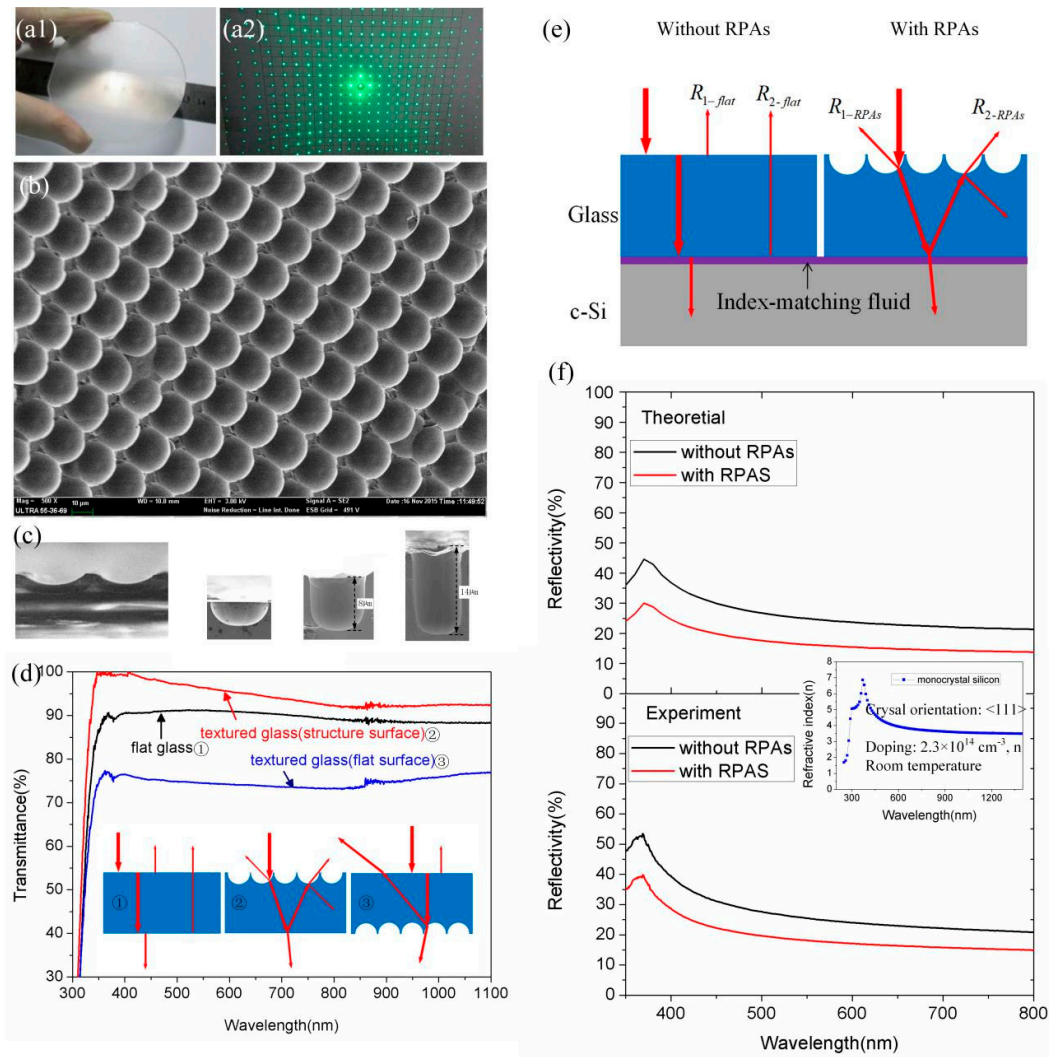


Figure 7. (a1,a2) Photograph of quasi-hemispherical pit array textured glass and its diffraction pattern with the laser beam (500 nm) passing through. (b) SEM image with RHPA array structure with 30-degree inclination. (c) SEM images of the pits with different aspect ratios. (d) Comparison of reflectivity spectrum of flat and textured glass samples. (e) Diagrammatic sketch for light reflectivity of the silicon wafer covered by the plane glass and the pit-array-structured glass. (f) The reflectivity curves of a silicon wafer with or without RHPA structure and RHPA-structured glass. The inset is the silicon reflectance graph, which is used in the theoretical calculations.

The theoretical and experimental results were compared digitally by using the following formulas to calculate the total reflectance $\langle R \rangle$ and relatively reduction ΔR :

$$R = \frac{1}{\lambda_2 - \lambda_1} \int_{\lambda_1}^{\lambda_2} r(\lambda) d\lambda \text{ and } \Delta R = \frac{R_{flat\ glass} - R_{RPAs-glass}}{R_{flat\ glass}} \quad (10)$$

where $r(\lambda)$ represents the theoretical or experimental values as a function of λ , $\lambda_1 = 350$ nm, and $\lambda_2 = 800$ nm. Table 1 shows the comparison results between the theory and the experiment. The theoretical and experimental results of ΔR are 32.95% and 29.64%, respectively, indicating that the RHPA structure can effectively decrease the reflectance of the silicon wafer by about 30%. Although the experimental values are lower than the theoretical values, these discrepancies are caused by the glass used in the experiment. In theoretical calculations, silicon is an ideal semiconductor material, and the designed glass sample is regarded as an ideal shape with a smooth plane and perfect hemispherical pits. How-

ever, in the experimental measurement, the surface of the prepared glass sample was not completely smooth, and the cut pits had a hemispherical-like structure. In addition, the refractive index of silicon may not be consistent with the theoretical refractive index. Therefore, the method for analyzing the light-trapping characteristics of RHPAs in this study is reasonable.

Table 1. The values of $\langle R \rangle$ and ΔR under the conditions of theory and experiment.

	$\langle R \rangle$		ΔR
	Flat	RHPAs	
Theory	26.28%	17.62%	32.95%
Experiment	28.51%	20.06%	29.64%

Both the experimental and theoretical results effectively express the pit array texture with good light-trapping properties. The decrease in surface reflectivity indicates an increase in light energy in the solar cell. In other words, the utilization of sunlight is improved. The photoelectric transformation efficiency for solar cell needs to be enhanced, especially for silicon thin-film solar cells.

5. Conclusions

The light-trapping characteristics of regular pit arrays with different aspect ratios in Si solar cells were studied. Numerical analysis and geometrical optics simulation were used to study the antireflection characteristics of the cell surface, the total light reflectivity, and the path length. The theoretical research results were verified using the micro/nano manufacturing method to obtain the flat and the quasi-hemisphere pit array glass samples. For the hemisphere pit arrays, theoretical derivation results indicate that it can reduce surface reflectance by more than half and can cause one third of the unabsorbed light to return to the active layer of the solar cell. Furthermore, the total optical path length for the cells with RHPAs increased from 2ω to 4ω , thus providing a favorable space for reducing the active layer thickness and saving manufacturing expense for cells. Simultaneously, regular pit arrays inhibited the inside light from escaping from the solar cells and returned the unabsorbed light back to the active layer. Thus, regular pit arrays have outstanding AR capability, which could decrease the total reflectivity for solar cells. The research in this article not only helps us to delve deeper into the mechanism of light-trapping, but also provides a reference for improving and researching more effective light-trapping structures. At the same time, it also has significant implications for the design of trapping structures for various optoelectronic devices.

Author Contributions: B.Z. and L.C. conceived the idea and supervised the project. B.Z. and S.Y. designed the simulation experiments, put forward the theoretical model, and contributed to the theoretical calculations. W.L. analyzed the data. B.Z. and L.C. wrote the manuscript. All authors have read and agreed to the published version of the manuscript.

Funding: This research is supported by the Guangxi Science and Technology Base and Talent Project (Department of Science and Technology of Gaungxi, Grant No.AD20297041), the Director’s Fund of Guangxi Key Laboratory of Automatic Testing Technology and Instruments (Guangxi Key Laboratory of Automatic Detection Technology and Instruments, Grant No.YQ21106), the National Natural Science Foundation of China (National Natural Science Foundation of China, Grant No.61804097), and the Guangxi Special Expert Team Project.

Data Availability Statement: The raw/processed data cannot be shared at this time as the data also forms part of an ongoing study.

Conflicts of Interest: The authors declare no conflict of interest.

References

1. Liu, H.; Du, Y.; Yin, X.; Bai, M.; Liu, W. Micro/Nanostructures for Light Trapping in Monocrystalline Silicon Solar Cells. *J. Nanomater.* **2022**, *2022*, 8139174. [[CrossRef](#)]
2. Tang, Q.; Yao, H.; Xu, B.; Ge, J. Enhanced energy conversion efficiency of Al-BSF c-Si solar cell by a novel hierarchical structure composed of inverted pyramids with different sizes. *Sol. Energy* **2020**, *208*, 1–9. [[CrossRef](#)]
3. Tang, Q.; Shen, H.; Yao, H.; Gao, K.; Ge, J.; Liu, Y. Investigation of optical and mechanical performance of inverted pyramid based ultrathin flexible c-Si solar cell for potential application on curved surface. *Appl. Surf. Sci.* **2020**, *504*, 144588. [[CrossRef](#)]
4. Lee, Y.; Woo, Y.; Lee, D.-K.; Kim, I. Fabrication of quasi-hexagonal Si nanostructures and its application for flexible crystalline ultrathin Si solar cells. *Sol. Energy* **2020**, *208*, 957–965. [[CrossRef](#)]
5. Liu, X.; Ji, Y.; Lu, Z.; Sun, Y.; Yang, H.; Liu, J.; Zhang, Y.; Li, D.; Cao, Y.; Li, W.; et al. Enhanced device performance of Si nanowires/Si nanocrystals heterojunction solar cells with ultrathin Al₂O₃ passivation. *Phys. E Low-Dimens. Syst. Nanostruct.* **2020**, *120*, 114048. [[CrossRef](#)]
6. Kordrostami, Z.; Sheikholeslami, H. Optimization of light trapping in square and hexagonal grid inclined silicon nanowire solar cells. *Opt. Commun.* **2020**, *459*, 124980. [[CrossRef](#)]
7. Seo, M.; Yoon, S.; Cho, H.; Lee, S.; Kim, K.; Kong, B.D.; Meyyappan, M.; Baek, C.-K. Solar Cell Using Hourglass-Shaped Silicon Nanowires for Increased Light-Trapping Path. *IEEE J. Photovolt.* **2020**, *10*, 475–479. [[CrossRef](#)]
8. Yamada, Y.; Iizuka, H.; Mizoshita, N. Silicon Nanocone Arrays via Pattern Transfer of Mushroomlike SiO₂ Nanopillars for Broadband Antireflective Surfaces. *ACS Appl. Nano Mater.* **2020**, *3*, 4231–4240. [[CrossRef](#)]
9. Le, C.; Bowen, F.; Qinglin, K.; Wangyang, P.; Hu, K.; Zhang, W. Quasi-hemispherical pit array textured surface for increasing the efficiency of thinfilm solar cells. *AIP Adv.* **2022**, *12*, 015111.
10. Xing, Y.P.; Zhang, K.L.; Zhao, J.S.; Han, P.D.; Yang, Z.C.; Yuan, Y.J.; Ding, Q. Antireflection and absorption properties of silicon parabolic-shaped nanocone arrays. *Optik* **2017**, *128*, 133–138. [[CrossRef](#)]
11. Chen, L.; Luo, W.; Fang, B.; Zhu, B.; Zhang, W. Study on light absorption of CH₃NH₃PbI₃ perovskite solar cells enhanced by gold nanopyramids. *Opt. Laser Technol.* **2023**, *159*, 108924. [[CrossRef](#)]
12. Xu, Z.; Huangfu, H.; Li, X.; Qiao, H.; Guo, W.; Guo, J.; Wang, H. Role of nanocone and nanohemisphere arrays in improving light trapping of thin film solar cells. *Opt. Commun.* **2016**, *377*, 104–109. [[CrossRef](#)]
13. Wang, C.; Zhao, S.; Bian, F.; Du, D.; Wang, C.; Xu, Z. Absorption enhancement of ultrathin crystalline silicon solar cells with frequency upconversion nanosphere arrays. *Commun. Theor. Phys.* **2020**, *72*, 015501. [[CrossRef](#)]
14. Chang, Y.-C.; Pollard, M.E.; Payne, D.N.R.; Sprafke, A.; Pillai, S.; Bagnall, D.M. Large-area nanosphere gratings for light trapping and reduced surface losses in thin solar cells. *IEEE J. Photovolt.* **2019**, *9*, 1012–1019. [[CrossRef](#)]
15. Chen, L.; Wang, Q.; Chen, W.; Liu, D.; Zhao, Z.; Wang, D. Light trapping mechanism of hemisphere cone arrays for silicon solar cells. *Sol. Energy* **2018**, *163*, 519–525. [[CrossRef](#)]
16. Zhang, C.; Guney, D.O.; Pearce, J.M. Plasmonic enhancement of amorphous silicon solar photovoltaic cells with hexagonal silver arrays made with nanosphere lithography. *Mater. Res. Express* **2016**, *3*, 105034. [[CrossRef](#)]
17. Khezami, L.; Al Megbel, A.O.; Jemai, A.B.; Ben Rabha, M. Theoretical and experimental analysis on effect of porous silicon surface treatment in multicrystalline silicon solar cells. *Appl. Surf. Sci.* **2015**, *353*, 106–111. [[CrossRef](#)]
18. Ben Rabha, M.; Mohamed, S.B.; Dimassi, W.; Gaidi, M.; Ezzaouia, H.; Bessais, B. Optoelectronic enhancement of monocrystalline silicon solar cells by porous silicon-assisted mechanical grooving. *Phys. Status Solidi C* **2011**, *8*, 887–890. [[CrossRef](#)]
19. Eduardo, C.A.; Hannah, J.J. Transparent Quasi-Random Structures for Multimodal Light Trapping in Ultrathin Solar Cells with Broad Engineering Tolerance. *ACS Photonics* **2022**, *9*, 2724–2735.
20. Senthilkumar, N.; Arulraj, A.; Nandhakumar, E.; Ganapathy, M.; Vimalan, M.; Potheher, I.V. Green mediated synthesis of plasmonic nanoparticle (Ag) for antireflection coating in bare mono silicon solar cell. *J. Mater. Sci. Mater. Electron.* **2018**, *29*, 12744–12753. [[CrossRef](#)]
21. Voroshilov, P.M.; Simovski, C.R.; Belov, P.A.; Shalin, A.S. Light-trapping and antireflective coatings for amorphous Si-based thin film solar cells. *J. Appl. Phys.* **2015**, *117*, 203101. [[CrossRef](#)]
22. Elshorbagy, M.H.; Abdel-Hady, K.; Kamal, H.; Alda, J. Broadband anti-reflection coating using dielectric Si₃N₄ nanostructures. Application to amorphous-Si-H solar cells. *Opt. Commun.* **2017**, *390*, 130–136. [[CrossRef](#)]
23. Kephart, J.M.; Geisthardt, R.M.; Sampath, W.S. Optimization of CdTe thin-film solar cell efficiency using a sputtered, oxygenated CdS window layer. *Prog. Photovolt. Res. Appl.* **2015**, *23*, 1484–1492. [[CrossRef](#)]
24. Rosell, A.; Martin, I.; Garin, M.; Lopez, G.; Alcubilla, R. Textured PDMS Films Applied to Thin Crystalline Silicon Solar Cells. *IEEE J. Photovolt.* **2019**, *10*, 351–357. [[CrossRef](#)]
25. Gao, Z.; Lin, G.; Chen, Y.; Zheng, Y.; Sang, N.; Li, Y.; Chen, L.; Li, M. Moth-eye nanostructure PDMS films for reducing reflection and retaining flexibility in ultra-thin c-Si solar cells. *Sol. Energy* **2020**, *205*, 275–281. [[CrossRef](#)]
26. Chen, G.; Hu, D.Q.; Li, C.; Wang, W.W.; Zhang, J.Q.; Wu, L.L.; Li, W. Process study about silica anti-reflection coatings prepared by sol-gel method for cadmium telluride solar cells. *J. Mater. Sci.* **2018**, *53*, 15588–15599. [[CrossRef](#)]
27. Zhang, C.; Song, Y.; Wang, M.; Yin, M.; Zhu, X.F.; Tian, L.; Wang, H.; Chen, X.Y.; Fan, Z.Y.; Lu, L.F.; et al. Efficient and Flexible Thin Film Amorphous Silicon Solar Cells on Nanotextured Polymer Substrate Using Sol-gel Based Nanoimprinting Method. *Adv. Funct. Mater.* **2017**, *27*, 1604720. [[CrossRef](#)]

28. Jannat, A.; Lee, W.; Akhtar, M.S.; Li, Z.Y.; Yang, O.B. Low cost sol-gel derived SiC-SiO₂ nanocomposite as anti reflection layer for enhanced performance of crystalline silicon solar cells. *Appl. Surf. Sci.* **2016**, *369*, 545–551. [[CrossRef](#)]
29. Kim, K.; Kim, S.; An, S.; Lee, G.H.; Kim, D.; Han, S. Anti-reflection porous SiO₂ thin film deposited using reactive high-power impulse magnetron sputtering at high working pressure for use in a-Si:H solar cells. *Sol. Energy Mater. Sol. C* **2014**, *130*, 582–586. [[CrossRef](#)]
30. Liu, D.; Wang, Q. Light-trapping surface coating with concave arrays for efficiency enhancement in amorphous silicon thin-film solar cells. *Opt. Commun.* **2018**, *420*, 84–89. [[CrossRef](#)]
31. Ashish, P.; Jordi, L.; Patricia, C.S. Broadband and Omnidirectional Antireflection Surfaces Based on Deep Subwavelength Features for Harvesting of the Solar Energy. *Sol. RRL* **2021**, *5*, 2100548.
32. Shen, X.Q.; Wang, Q.K.; Wangyang, P.H.; Huang, K.; Chen, L.; Liu, D.M. Performance enhancement in a-Si:H/ μ c-Si:H tandem solar cells with periodic microstructured surfaces. *Opt. Lett.* **2015**, *40*, 1290–1293. [[CrossRef](#)] [[PubMed](#)]
33. Jovanov, V.; Palanchoke, U.; Magnus, P.; Stiebig, H.; Hüpkes, J.; Sicanugrist, P.; Konagai, M.; Wiesendanger, S.; Rockstuhl, C.; Knipp, D. Light trapping in periodically textured amorphous silicon thin film solar cells using realistic interface morphologies. *Opt. Express* **2013**, *21*, A595–A606. [[CrossRef](#)]
34. Tamang, A.; Pathirane, M.; Parsons, R.; Schwarz, M.M.; Iheanacho, B.; Jovanov, V.; Wagner, V.; Wong, W.S.; Knipp, D. Zinc oxide nanowire arrays for silicon core/shell solar cells. *Opt. Express* **2014**, *22*, A622–A632. [[CrossRef](#)]
35. Preinfalk, J.B.; Donie, Y.J.; Egel, A.; Hecht, M.; Hüpkes, J.; Bittkau, K.; Lemmer, U.; Gomard, G. On the fabrication of disordered nanostructures for light extraction in corrugated OLEDs. In *Solid-State Lighting*; Optica Publishing Group: Washington, DC, USA, 2017; p. JW5A.20.
36. Yablonovitch, E. Statistical ray optics. *JOSA* **1982**, *72*, 899–907. [[CrossRef](#)]
37. Deckman, H.W.; Roslo, C.B.; Yablonovitch, E. Maximum statistical increase of optical absorption in textured semiconductor films. *Opt. Lett.* **1983**, *8*, 491–493. [[CrossRef](#)]
38. Nelson, J. *The Physics of Solar Cells*; Imperial College Press: London, UK, 2003; p. 223.
39. Available online: <https://refractiveindex.info/?shelf=main&book=Si&page=Aspnes> (accessed on 3 April 2022).
40. Aspnes, D.E.; Studna, A.A. Dielectric functions and optical parameters of Si, Ge, GaP, GaAs, GaSb, InP, InAs, and InSb from 1.5 to 6.0 eV. *Phys. Rev. B* **1983**, *27*, 959–1009. [[CrossRef](#)]

Disclaimer/Publisher’s Note: The statements, opinions and data contained in all publications are solely those of the individual author(s) and contributor(s) and not of MDPI and/or the editor(s). MDPI and/or the editor(s) disclaim responsibility for any injury to people or property resulting from any ideas, methods, instructions or products referred to in the content.